

DocGenome: An Open Large-scale Scientific Document Benchmark for Training and Testing Multi-modal Large Language Models

Renqiu Xia^{1,2,*}, Song Mao^{1,*}, Xiangchao Yan^{1,*}, Hongbin Zhou¹, Bo Zhang^{1,†}
Haoyang Peng¹, Jiahao Pi¹, Daocheng Fu¹, Wenjie Wu^{1,2}, Hancheng Ye¹, Shiyang Feng⁴
Bin Wang¹, Chao Xu¹, Conghui He¹, Pinlong Cai¹, Min Dou¹, Botian Shi^{1,‡}
Sheng Zhou³, Yongwei Wang³, Bin Wang⁴, Junchi Yan^{1,2}, Fei Wu³, Yu Qiao¹

¹ Shanghai Artificial Intelligence Laboratory, ² Shanghai Jiao Tong University
³ Zhejiang University, ⁴ Fudan University

Abstract

Scientific documents record research findings and valuable human knowledge, comprising a vast corpus of high-quality data. Leveraging multi-modality data extracted from these documents and assessing large models’ abilities to handle scientific document-oriented tasks is therefore meaningful. Despite promising advancements, large models still perform poorly on multi-page scientific document extraction and understanding tasks, and their capacity to process within-document data formats such as charts and equations remains under-explored. To address these issues, we present DocGenome, a structured document benchmark constructed by annotating 500K scientific documents from 153 disciplines in the arXiv open-access community, using our custom auto-labeling pipeline. DocGenome features four key characteristics: 1) *Completeness*: It is the first dataset to structure data from all modalities including 13 layout attributes along with their L^AT_EX source codes. 2) *Locality*: It provides 6 logical relationships between different entities within each scientific document. 3) *Diversity*: It covers various document-oriented tasks, including document classification, visual grounding, document layout detection, document transformation, open-ended single-page QA and multi-page QA. 4) *Correctness*: It undergoes rigorous quality control checks conducted by a specialized team. We conduct extensive experiments to demonstrate the advantages of DocGenome and objectively evaluate the performance of large models on our benchmark. DocGenome is available at https://unimodal4reasoning.github.io/DocGenome_page

1 Introduction

Extracting data from scientific documents and developing large models to understand them is crucial for advancing AI-assisted scientific exploration and discovery [19, 11, 4]. On one hand, scientific documents provide comprehensive, high-quality, logically rich corpora for training large models [31, 7, 8, 33]. On the other hand, the ability of large models [31, 7, 8, 33] to accurately understand scientific documents is considered as a crucial evaluation criterion.

However, we observed that current Multi-modal Large Language Models (MLLMs) [22, 54, 34, 9, 44, 7, 8, 5, 1, 23, 39, 45, 46, 48, 53, 56] still struggle to understand the content of scientific documents as deeply as humans do. This challenge is primarily due to the inherently complicated multi-modal information present in scientific documents, such as multi-modal charts [50], intricate equations [42], and sophisticated logical relationships. Currently, MLLMs cannot effectively parse

*Equal contribution, †Corresponding authors.

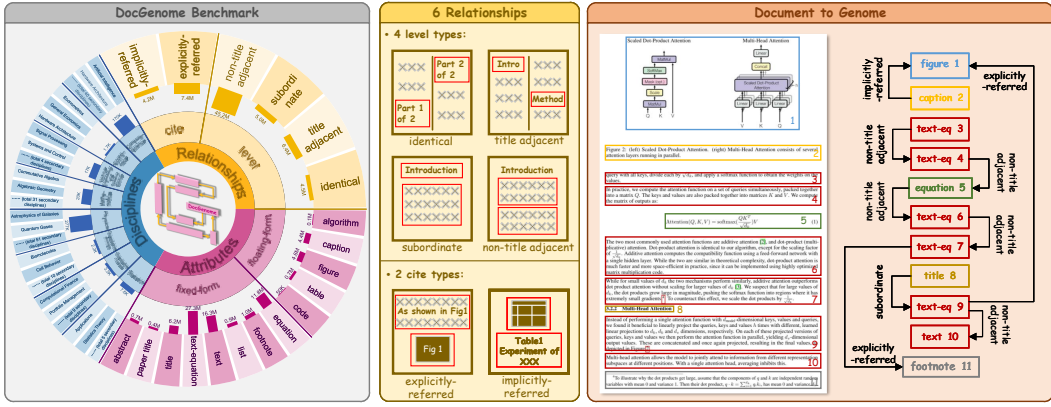


Figure 1: Overview of the DocGenome dataset. Our work introduces DocGenome, a multi-modal dataset of academic documents encompassing 8 primary disciplines, 153 secondary disciplines, 13 categories of component units, and 6 types of entity relationships between units. We showcase an example of the paper [41] parsing into structured graph forms, termed as the document’s genome, by leveraging the attributes and relationships of component units.

and comprehend such complicated modalities and logical relationships. To alleviate this challenge, we present DocGenome, an open large-scale scientific document benchmark constructed using the designed DocParser.

DocParser is a cutting-edge auto-labeling pipeline, which can generate both attribute information of component units and logical relationships between units by auto-annotating and structuring a large amount of unlabeled arXiv papers, with four stages: 1) data preprocessing, 2) unit segmentation, 3) attribute assignment and relation retrieval, and 4) color rendering as elaborated in Sec. 3.1. Furthermore, we utilize the proposed DocParser to label 500K scientific documents collected from the arXiv open-access community, and the resulting auto-annotated dataset is termed as DocGenome (illustrated in Fig. 1), which contains 153 scientific disciplines and 7 document-oriented tasks including: document classification, visual grounding, open-ended single-page and multi-page QA tasks, document layout detection, Equation-to-L^AT_EX transformation, Table-to-L^AT_EX transformation, which is elaborated in Sec. 4.3. Furthermore, we employ the quality grading and human validation methods to ensure the data quality as described in Sec. 3.2 and Sec. 4.2, respectively.

We conduct extensive experiments on the proposed DocGenome benchmark to objectively evaluate many mainstream MLLMs, including QWen-VL [5], CogAgent [15], InternVL 1.5 [8], GPT-4V [33], and *etc.* The experiments on DocGenome also verify the effectiveness of the proposed dataset, demonstrating its ability to enhance the document understanding of the existing baseline models.

Our main contributions can be summarized as follows:

- For the first time, we construct an open large-scale dataset that includes **500K** structured scientific documents with **13** categories of component units and **6** types of logical relationships between them. This dataset also encompasses various data types within scientific documents, such as Figure, Equation, Table, Algorithm, List, Code, Footnote, and *etc.*
- To construct DocGenome, we design DocParser to automatically generate rich annotation information from the source code of a wealth of arXiv papers.
- DocGenome covers **7** document-oriented tasks, such as document layout detection, document transformation, multi-page QA, *etc.* Besides, we conduct extensive verification and experiments based on these tasks to demonstrate that DocGenome can significantly enhance the document understanding capabilities of the existing baselines.

2 Related Works

Visual Document Datasets. To comprehensively show the advantages of the proposed DocGenome dataset, we have reviewed visual document datasets and summarized them in Table 1. In earlier years, visual document datasets [22, 54, 34, 9] mainly aim to recognize the region categories of different regions from a given document, such as text region, table region, abstract region, and *etc.* For example,

Table 1: Comparison with document-related benchmarks. “ - ” indicates that the corresponding part is not mentioned in the original paper. “ * ” means that each sample in their training set is cropped from the entire page, resulting in a total of 6.4M samples at the region level rather than the page level.

Datasets	# Discipline	# Category of Component Units	# Pages in Train-set	# Pages in Test-set	# Task Type	# Used Evaluation Metric	Publication Period	With-Entity Relation
DocVQA [32]	-	N/A	11K	1K	1	2	1960-2000	✗
DocLayoutNet [34]	-	11	80K	8K	1	1	-	✗
DocBank [22]	-	13	0.45M	50K	3	1	2014-2018	✗
PubLayoutNet [54]	-	5	0.34M	12K	1	1	-	✗
VRDU [47]	-	10	7K	3K	3	1	-	✗
DUDE [40]	-	N/A	20K	6K	3	3	1860-2022	✗
D^4LA [9]	-	27	8K	2K	1	3	-	✗
Fox Benchmark [25]	-	5	N/A (No train-set)		0.2K	3	5	✗
ArXivCap [21]	32	N/A	6.4M*		N/A	4	3	✗
DocGenome (ours)	153	13	6.8M	9K	7	7	2007-2022	✓

DocBank [22] constructs 500K high-quality document pages to enable the document layout model to utilize both textual and visual information. Recently, some research works [32, 49, 50, 40, 21, 25] are proposed to build a document dataset with the enhanced diversity from multiple tasks, multiple modalities, and large-scale training data. By comparison, our DocGenome demonstrates more comprehensive features, including the number of disciplines and training samples covered, types of tasks, evaluation metrics, and entity relationships.

Visual Document Understanding. Research in the field of document Artificial Intelligence (AI) has made rapid progress, due to its successful applications in visual document layout analysis [43, 40, 9, 3, 30, 17, 14] and image representation learning [55, 13, 10, 6]. Inspired by Transformer [41], LayoutLMv3 [17] utilizes word-patch features to perform pre-training and designs a cross-modal alignment for document AI. UDIO [37] tries to unify multiple document-oriented vision tasks using task-specific prompting. Besides, Kosmos-2.5 [31] generates the text outputs by a shared decoder-only Transformer. mPLUG-DocOwl [52] boosts the OCR-free document understanding ability. Recently, ICL-D3IE [12] proposes an in-context-based learning framework to integrate LLM into document information extraction tasks and LayoutLLM [30] employs the layout instruction mechanism to improve the ability of document analysis.

Multi-modal Large Language Models (MLLMs). The development of MLLMs has profound impacts on the Artificial General Intelligence (AGI) landscape. Recently, commercial MLLMs [33, 38, 2, 35] have experienced extremely rapid progress. GPT-4V [33] has significantly advanced the MLLMs. Google’s Genimi series [38, 35] further enhance the ability of MLLMs to process text, images, and audio. Besides, open-source MLLMs [44, 7, 8, 5, 1, 29, 23, 24, 27, 36, 39, 45, 46, 48, 53, 56] have also attracted great attention. Such MLLMs bring accessibility to the rapid development of AI, enabling widespread multi-modal applications and fostering innovation across industries.

3 Data Collection Methodology For DocGenome

3.1 Introduction of Auto-labeling Pipeline

In this section, we present DocParser, a cutting-edge auto-labeling pipeline that streamlines the extraction of labeled source code from unlabeled arXiv data, serving as a key instrument for annotating the DocGenome dataset. As shown in Fig. 2, the annotation process of DocParser is concisely divided into four stages, mitigating the issues of data scarcity and annotation expenses.

Stage 1: Data Preprocessing. Our primary focus is to improve the data quality and enhance the compilation success rate of \LaTeX source code. Initially, we undertake an expansion of all files referenced by the \input and \include commands, followed by a series of crucial pre-processing steps. These steps encompass the integration of requisite environment packages, the exclusion of comment lines, and the removal of extraneous tokens such as \vspace, \ref, and other annotations that do not contribute to the semantic essence of the document. Subsequently, we concentrate on standardizing the figure format within the \LaTeX source code, converting all graphical elements to the PNG format. Furthermore, we remove the color attribute from the “hyperref”, ensuring that the \LaTeX source code is ready for targeted color rendering during annotation in stage 4.

Stage 2: Units Segmentation. The objective of this phase is to automate the segmentation of content units, thereby streamlining the rendering process for distinct sections. We employ the

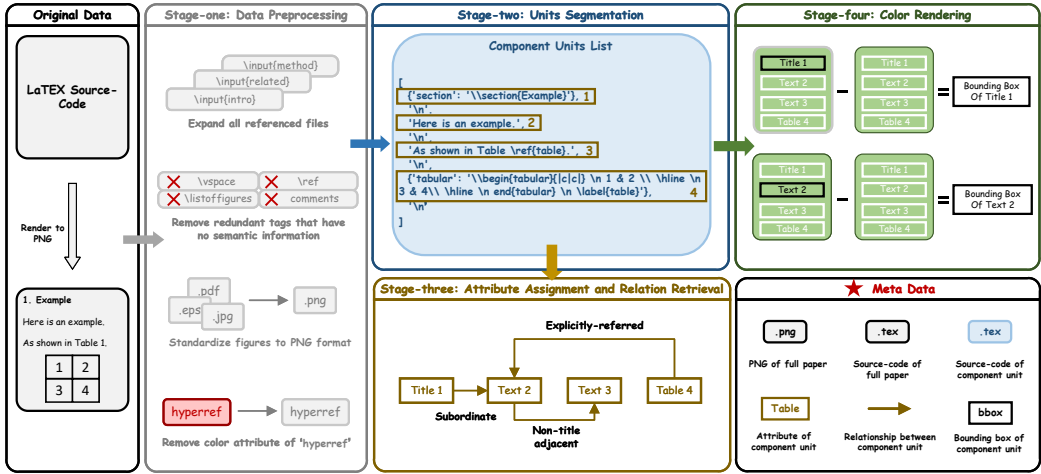


Figure 2: Schematic of the designed DocParser pipeline for automated document annotation. The process is divided into four distinct stages: 1) Data Preprocessing, 2) Unit Segmentation, 3) Attribute Assignment and Relation Retrieval, and 4) Color Rendering. DocParser can convert \LaTeX source code of a complete document into annotations for component units with source code, attributes, relationships, and bounding box, as well as a rendered PNG of the entire document.

Table 2: The definition of logical relationships between component units.

Relation Name	Specific Description	Example
<i>Identical</i>	Two units share the same source code.	Cross-column text; Cross-page text.
<i>Title adjacent</i>	The two titles are adjacent.	(\section{introduction}, \section{method})
<i>Subordinate</i>	One unit is a subclass of another unit.	(\section{introduction}, paragraph within Introduction)
<i>Non-title adjacent</i>	The two text or equation units are adjacent.	(Paragraph 1, Paragraph 2)
<i>Explicitly-referred</i>	One unit refers to another unit via footnote, reference, etc.	(As shown in \ref{Fig: 5} ..., Figure 5)
<i>Implicitly-referred</i>	The caption unit refers to the corresponding float environment.	(Table Caption 1, Table 1)

TexSoup[¶] library to decompose the \LaTeX source code into a structured list, delineating each individual component unit. This list is organized according to the reading order, ensuring a logical progression and facilitating the subsequent retrieval of relationships between the component units.

Stage 3: Attribute Assignment and Relation Retrieval. We have defined **13** fine-grained layout attributes (more details in Table A.1 of Appendix C) for the component units decomposed in Stage 2, encompassing elements such as Algorithms, Captions, Equations, etc. For each unit, we match an appropriate attribute from the predefined set using keyword queries and regularization techniques to ensure a tailored and precise categorization. In the analysis of component unit relationships, units are categorized into two classes: **1) fixed-form units**, including Text, Title, Abstract, etc., which are characterized by sequential reading and hierarchical relationships readily discernible from the list obtained in Stage 2, and **2) floating-form units**, including Table, Figure, etc., which establish directional references to fixed-form units through commands like `\ref` and `\label`. The comprehensive set of **6** entity relationships is detailed in Table 2.

Stage 4: Color Rendering. The bounding box of a component unit is an additional label we aim to extract. After the segmentation phase in Stage 2, we render the target unit in black and all other units in white, to create two distinct PDFs. By performing a subtraction operation between these documents, we can obtain the detection box containing only the current unit, as illustrated in the top-right corner of Fig. 2. For component units that traverse across hurdles or pages, we standardize the bounding box labels based on their unified source code information. This method effectively

[¶]TextSoup package: <https://github.com/alvinwan/TexSoup>.

mitigates the issue where bounding boxes may be inadvertently divided, ensuring seamless and unified labeling for such units.

We automate the annotation process by sequentially applying DocParser’s four stages and leveraging the complete L^AT_EX source code. This yields not only the document’s PDF but also the individual source code, bounding box, specific attributes for each component unit, and the relationships between units. Together, these elements constitute our DocGenome dataset.

3.2 DocGenome Benchmark Analyses

Utilizing the DocParser automated annotation tool, we have annotated a corpus comprising 500K academic articles from the arXiv repository. Our analysis explores the diversity of the DocGenome benchmark, focusing on discipline distribution, content distribution, and quality grading.

Discipline Distribution. The DocGenome consists of 8 primary disciplines, which collectively encompass 153 secondary disciplines¹, reflecting a diverse and extensive coverage of academic research areas. The distribution across these disciplines is detailed in Fig. A.2 of Appendix D.

Year Distribution. DocGenome archives articles from arXiv, ranging from 2007 to 2022, with a median publication year of 2016. A significant portion, approximately 32.88%, of these articles have been published since 2020. The distribution of these publications over time is depicted in Fig. 3a.

Content Distribution. We have examined two key aspects: the distribution of page counts and the labeling of component units. On the dimension of page counts, the dataset’s documents have an average page count of 13, with the longest document reaching 50 pages. The distribution of page counts is graphically represented in Fig. A.1 of Appendix C. Moving to the labeling perspective, we have annotated a substantial collection of 500K documents, totaling 74.5M component units and 68.5M relationship labels. In Fig. 1, we present a detailed visualization of the distribution of both the attribute tags of the component units and the relationship labels.

Quality Grading. We establish two metrics to grade the data quality of the auto-labeled data that are generated using our DocParser. The first metric, designated as Eq. 1, measures the overlap among auto-annotated bounding boxes within each paper, thereby evaluating the intra-consistency of annotations:

$$IoU_{\text{intra}} = \frac{1}{N(N-1)} \sum_{i=1}^N \sum_{j=1, j \neq i}^N J(B_i, B_j), \quad (1)$$

where $J(B_i, B_j) = \frac{O(B_i, B_j)}{A(B_i) + A(B_j) - O(B_i, B_j)}$ is the IoU between bounding boxes B_i and B_j . N is the total number of annotated bounding boxes in each paper. $O(B_i, B_j)$ represents the overlap area between bounding boxes B_i and B_j . $A(\cdot)$ refers to the area of the bounding box.

Eq. 2 shows the second metric that quantifies the overlap between these annotated bounding boxes and the reference bounding boxes (predicted by DocXChain [51]), providing an assessment of the annotations’ alignment with established benchmarks, as formulated in Eq. 2:

$$IoU_{\text{align}} = \frac{1}{N} \sum_{i=1}^N J(B_i, G_i), \quad (2)$$

where G_i is the i -th reference bounding box generated by DocXChain [51], B_i refers to the bounding box that is closest to G_i within our annotated ones.

A lower IoU_{intra} with a higher IoU_{align} indicates a higher quality of auto-annotated bounding boxes. Specifically, we split the collected paper into three tiers based on the annotation results. For the *Tier-1* set, we select the papers with $IoU_{\text{intra}} < 0.05\%$ and $IoU_{\text{align}} > 60\%$, while those with $0.05\% \leq IoU_{\text{intra}} < 1\%$ and $IoU_{\text{align}} > 35\%$ are packed in the *Tier-2* set, and the remaining papers are categorized as the *Tier-3* set. The distribution of three-tier data sets is shown in Fig. 3b, indicating that 28.56% of the data was allocated to *Tier-1*, 61.30% to *Tier-2*, and the other 10.14% to *Tier-3*.

¹According to the arXiv Category Taxonomy: https://arxiv.org/category_taxonomy.

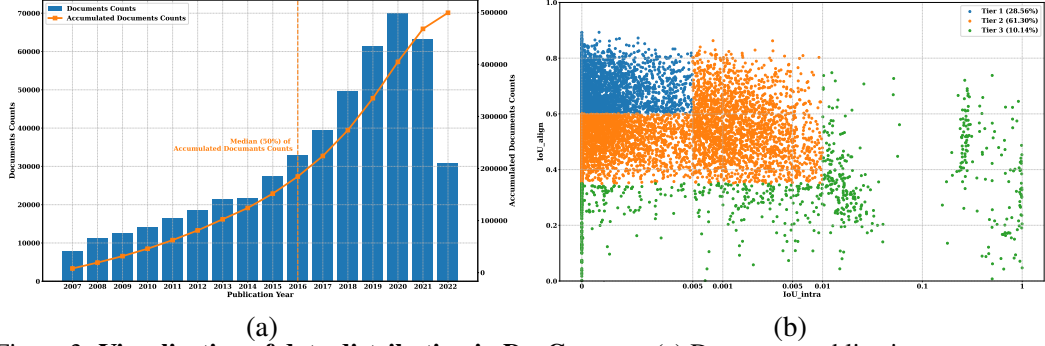


Figure 3: **Visualization of data distribution in DocGenome.** (a) Document publication counts over the years. (b) Distribution of three *Tiers* determined by IoU_{intra} and IoU_{align} .

4 DocGenome-test: A Multi-task, Multi-modal, Comprehensive Evaluation Set for Document Understanding

4.1 Principles of Constructing Evaluation Set

We use two principles to split the auto-annotated data into a high-quality evaluation set (**termed as DocGenome-test**) with precise annotation and a large-scale multi-modal training set (**termed as DocGenome-train**). First, the evaluation set should share the same discipline distribution as the collected data. Hence, the test data are uniformly sampled across each discipline. Second, the annotation of test data should be as precise as possible. Therefore, the test data are only sampled from the *Tier-1* set. Based on these two principles, we finally sampled 1,004 papers (covering 9K pages) as the test set from the overall 500K auto-annotated papers (containing 6.8M pages). As a result, the DocGenome-test covers 1,004 scientific documents with 1K document classification examples, 2K visual grounding examples, 3K QA pairs, 110K layout bounding boxes, 3K Table-L^AT_EX pairs, and 5K Equation-L^AT_EX pairs.

4.2 QA Pair Generation and Quality Assurance

In the DocGenome-test, we further design multiple Question-Answering (QA) pairs for each paper to comprehensively evaluate the document understanding capabilities of different models. For each paper sampler, two single-page QA pairs and two multi-page QA pairs are generated using GPT-4V [33]. Specifically, we instruct GPT-4V to randomly select two representative pages, extract useful information from the two pages respectively, and then generate corresponding single-page QA pairs. Additionally, we utilize GPT-4V to search for content-related paragraphs from different pages to construct the cross-page QA pairs, testing the model’s ability to understand and integrate information across multiple pages. The QA pairs involve various commonly raised questions whose answers can be precisely inferred from the given paper.

After generating QA pairs for all paper samples in the DocGenome-test, we invited professional faculty members from various fields to conduct the quality assurance checks. Each QA pair is reviewed by three reviewers for cross-verification. The first step involves the initial review by Kimi^{††}, a well-known paper understanding model, to assess the initial correctness and identify the target location of QA information on the assigned page. Next, based on the provided location of QA information, two professional faculty members are assigned to manually and independently check each QA pair for accuracy, relevance, and clarity. At this stage, the quality evaluation involves the correctness, relevance, and rationality of the designed questions and the accuracy of the provided answer. Finally, the two manually-evaluated results, along with the automatically-evaluated result are cross-verified with the original text to ensure accuracy and consistency. Please refer to Appendix E for more details.

^{††}Kimi online API: <https://kimi.moonshot.cn>.

Table 3: Comparison of state-of-the-art multi-modal large language models on the proposed DocGenome-test, including document classification, visual grounding, open-ended single-page, and multi-page QA tasks. Please refer to Sec. 4.4 for the employed evaluation metrics.

Model	#Params	Classification Acc↑	Visual Grounding		Document QA	
			Title Edit Distance↓	Abstract Edit Distance↓	Single-Page GPT-acc↑	Multi-Page GPT-acc↑
<i>Multi-modal Large Language Models</i>						
QWen-VL [5]	9.6B	0.8237	0.0775	0.8054	0.1156	0.0627
CogAgent [15]	17.3B	0.5857	0.0166	0.5306	0.1772	-
DocOwl-1.5 [16]	8.1B	0.3307	0.0509	0.6555	0.3084	-
Text-Monkey [26]	10B	0.7331	0.0371	0.4551	0.1142	-
IntenVL 1.5 [8]	26B	0.7590	0.0222	0.3601	0.4529	0.3577
GPT-4V [33]	N/A	0.9801	0.0104	0.4730	0.6101	0.6501

4.3 Evaluation Tasks

To comprehensively evaluate the models’ understanding capability of scientific documents, we design 7 tasks *w.r.t* each paper document for the DocGenome-test, including document classification, visual grounding, open-ended single-page, and multi-page QA tasks, document layout detection, Equation-to-LATEX transformation, and Table-to-LATEX transformation.

Specifically, document classification involves recognizing the field to which a paper belongs. Visual grounding involves identifying the content according to the provided visual components and textual prompts. Document layout detection refers to the localization and recognition of each layout block in given papers. Document transformation encompasses two format conversions, *i.e.*, Table-to-LATEX and Equation-to-LATEX transformation. All tasks take the paper images as visual input for inference. The visual examples for each task are illustrated in Fig. A.8 in Appendix H.

4.4 Evaluation Metrics

Document Classification: Top-1 Accuracy (%) is used as the metric for document classification tasks, where higher values indicate better performance.

Visual Grounding: Edit Distance is used to evaluate the accuracy of visual grounding, with lower values indicating better performance.

Document Layout Detection: mAP@0.5:0.95 is evaluated as the metric for document layout detection, where higher values indicate better performance.

Document Transformation: We utilize Edit Distance, Jaccard Similarity, Cosine Similarity, and BLEU as metrics to comprehensively evaluate the document transformation task.

Open-ended QA: GPT-acc (%) is designed for tasks with open-ended answers, where outputs are evaluated against the ground truth using GPT-4. Please refer to Appendix F for more details.

5 Experiments

5.1 Compared Baselines and Implementation

Compared Baselines. We select various models as baselines for different tasks to provide comprehensive comparisons. Specifically, various multi-modal language models, *e.g.*, QWen-VL [5], CogAgent [15], DocOwl-1.5 [16], Text-Monkey [26], IntenVL 1.5 [8], and GPT-4V [33] are tested on document classification, visual grounding, open-ended single-page QA and multi-page QA tasks. For the Document Layout Detection task, we compare DocXChain [51] and YOLOv8 [18]. Additionally, we employ Mathpix, a representative commercial software for mathematical formula transformation, as the compared method for the Document Transformation task, including Equation-to-LATEX and Table-to-LATEX transformations.

Implementation Details. We utilize a combination of document images and instruction prompts as the input. Note that all tasks use a single-page document image as the input, except for the multi-page QA task, which contains at least two consecutive pages of the document. Besides, the multi-page QA task can only be evaluated on the models that support multi-image inputs. For the layout detection task, which uses the single-page document image as input, we use YOLOv8 [18] as the training baseline, trained for 30 epochs with the AdamW optimizer [28], with a learning rate of 0.01. For Equation-to-LATEX and Table-to-LATEX tasks, we first use the layout annotations to crop out different modalities, *e.g.*, Table, Equation, *etc.*, from the original images. We then employ the same model

Table 4: Experiments on scaling up the data using the DocGenome-train, with the resulting models evaluated on document layout detection task. We fine-tune YOLOv8 [18] model using the DocGenome-train with different amounts of training data.

Model	Training Data Amount	mAP@0.5:0.95↑	Title	Text	Figure	Caption	Equation	Table	Footnote
<i>Layout detection task on DocGenome-test</i>									
DocXChain [51]	N/A	53.20	49.21	79.22	43.85	48.18	49.36	72.79	29.79
YOLOv8 [18]	7K	77.47	71.79	92.48	76.29	86.56	80.65	85.81	48.43
YOLOv8 [18]	70K	89.42	83.46	95.56	86.36	94.92	90.13	92.77	82.72
YOLOv8 [18]	700K	91.37	86.05	95.96	88.46	95.71	93.06	93.77	86.52

Table 5: Experiments on scaling up the data using the DocGenome-train, with the resulting models evaluated on equation and table transformation tasks. EqVLM-B and TableVLM-B mean that we train a visual encoder and a text decoder using the DocGenome-train for the equation and table transformation task, respectively.

Model	Training Data Amount	Edit Distance↓	Jaccard Similarity↑	Cosine Similarity↑	BLEU↑
<i>Equation-to-LaTeX task on DocGenome-test</i>					
Mathpix [‡]	N/A	0.4738	0.7226	0.6045	0.4472
EqVLM-B	10K	0.3781	0.8157	0.7840	0.5165
EqVLM-B	100K	0.2795	0.8505	0.8317	0.5862
EqVLM-B	1M	0.2111	0.8736	0.8621	0.6352
<i>Table-to-LaTeX task on DocGenome-test</i>					
Mathpix [§]	N/A	0.4436	0.7730	0.5826	0.3528
TableVLM-B	5K	0.4821	0.8158	0.7804	0.4596
TableVLM-B	10K	0.4738	0.8635	0.8187	0.4973
TableVLM-B	100K	0.3091	0.8903	0.8571	0.5340
TableVLM-B	500K	0.2223	0.8997	0.8800	0.5552

structure as Pix2Struct-B (0.2B parameters) [20] to perform the fine-tuning on DocGenome-train, resulting in EqVLM-B and TableVLM-B. The fine-tuning process lasts for 30 epochs on 64 NVIDIA A100 80G GPUs, with an initial learning rate of 0.00005 and a weight decay of 0.01.

5.2 Performance on DocGenome-test

We evaluate the performance of several state-of-the-art multi-modal large language models on the proposed DocGenome-test, covering document classification, visual grounding, and both single-page and multi-page QA tasks. As shown in Table 3, among the tested models, GPT-4V [33] achieves the highest classification accuracy with 98.0% Top-1 Acc, while QWen-VL [5] and InternVL 1.5 [8] also show competitive results with 82.4% and 75.9% accuracy, respectively. For the visual grounding task, GPT4V showcases the best performance in the Title OCR Grounding task with the lowest Edit Distance of 0.0104, while InternVL 1.5 outperforms other models in the Abstract OCR Grounding task with the lowest Edit Distance of 0.3601. In the single-page QA task, GPT-4V attains the highest GPT-acc score of 61.0%, indicating its superior ability to handle document-based QA tasks. For the multi-page QA task, GPT-4V again leads with a GPT-acc score of 65.0%, further demonstrating its robustness in handling multi-page document queries.

5.3 Effectiveness of DocGenome-train

To validate the effectiveness of the proposed DocGenome-train, we further conduct experiments on scaling up the training data using the DocGenome-train dataset, evaluating the performance improvements of different tasks, *e.g.*, layout detection and document transformation tasks.

Specifically, for the layout detection task, we present the evaluation performance of YOLOv8 [18] under three different training scales in Table 4. It shows that the model’s layout detection capacity continually and significantly improves by increasing the training data volume. Regarding the per-attribute performance improvement, the most significant benefit is observed for “Footnote” attribute, which increases from 48.43% to 86.52% mAP after scaling up the training data from 7K to 700K. Compared with DocXChain [51] that only supports the annotation of seven attributes, our trained YOLOv8 consistently outperforms it in seven attributes, validating the effectiveness of the DocGenome-train.

As illustrated in Table 5, for the document transformation task, we conduct similar experiments on Equation-to-LATEX task and Table-to-LATEX task, respectively. In these two tasks, we further explore

Table 6: Comparisons with state-of-the-art tools on Out-Of-Distribution (OOD) data, where Mathpix is a closed-source commercial software that requires a subscription, while ours is an open-source and free tool.

Model	mAP@0.5:0.95↑	Title	Text	Figure	Caption	Equation	Table	Footnote
<i>Layout detection task on Human-annotated data</i>								
DocXChain [51]	37.99	32.53	59.00	67.17	38.71	12.98	38.99	16.54
YOLOv8 [18]	50.15	42.59	64.87	56.65	64.51	47.14	47.08	28.21
<i>Equation-to-LaTeX task on Sci-Hub data</i>								
Mathpix [‡] .				0.4873	0.7437	0.7295	0.1137	
EqVLM-B				0.6627	0.6303	0.5726	0.0602	

different scaling up settings, with the observation that both tasks benefits the most from scaling up training data from 10K to 100K. Additionally, considering that Edit Distance is more reliable and rigorous to evaluate the similarity, we can observe that the Table-to-LATEX task has the potential to improve more than the Equation-to-LATEX task by continuous scaling up. This is because the performance improvement between 100K and 500K training data for TableVLM-B largely exceeds the improvement between 100K and 1M training data for EqVLM-B as shown in Table 5.

5.4 Further Discussions

Generalization on Out-Of-Distribution (OOD) Data. We discuss the generalization ability of models trained on our DocGenome-train to OOD data. Specifically, we conduct experiments on human-annotated data for the layout detection task and Scihub data for the Equation-to-LATEX task. As shown in Table 6, for the layout detection task, YOLOv8 [18] trained using DocGenome-train presents better generalization ability than DocXChain on human-annotated data. Regarding the Equation-to-LATEX task, although the performance of EqVLM-B declines on OOD data (Scihub data), it still maintains relatively strong results with an Edit Distance of 0.6627. Considering that Mathpix is a closed-source tool with potential exposure to various data distributions in its commercial usage, it is natural that our trained model performs relatively worse than Mathpix in the OOD data.

Potential Applications of DocDenome. 1) Conducting document transformation task for more modality types: DocGenome includes various types of data within scientific documents, such as Charts, Equations, Tables, Algorithms, Lists, Codes, and Footnotes, etc. For this paper, we study the document transformation using only two types of modalities: Table-to-LATEX and Equation-to-LATEX. Similarly, we can also train a model (image-encoder followed by a text-decoder) that can address the Algorithm-to-LATEX or List-to-LATEX transformation task, etc using DocGenome.

- 2) Performing document-level tasks with entity relations: DocGenome contains the logical relationships between component units, we can input different component units to examine the model’s understanding of long-range contextual relationships.
- 3) Conducting document OCR task on any page at any location: the layout annotations of DocGenome are very comprehensive, covering almost all locations in the document, and DocGenome has the ground truth text of the entire document. Therefore, we can use the layout information and text information to perform OCR tasks on any page at any location, not just the title and abstract regions, which further examines both the OCR capability and the visual grounding capability of the model.

6 Conclusion

In this paper, we introduced DocGenome, a large-scale, structured, multi-task, and multi-modal dataset for scientific documents. We constructed DocGenome using DocParser, our developed auto-labeling pipeline, to extract structured attributes and relationships between units. DocGenome’s comprehensive task coverage, logicality, diversity, and correctness make it a valuable resource for training models related to scientific documents and evaluating the capabilities of such large models.

Acknowledgement

The research was supported by the National Key R&D Program of China (Grant No. 2022ZD0160104), the Science and Technology Commission of Shanghai Municipality (Grant No. 22DZ1100102), and Shanghai Rising Star Program (Grant No. 23QD1401000).

References

- [1] Jean-Baptiste Alayrac, Jeff Donahue, Pauline Luc, Antoine Miech, Iain Barr, Yana Hasson, Karel Lenc, Arthur Mensch, Katherine Millican, Malcolm Reynolds, et al. Flamingo: a visual language model for few-shot learning. *Advances in neural information processing systems*, 35:23716–23736, 2022.
- [2] Anthropic. The claude 3 model family: Opus, sonnet, haiku. <https://www.anthropic.com>, , 2024.
- [3] Srikanth Appalaraju, Peng Tang, Qi Dong, Nishant Sankaran, Yichu Zhou, and R Manmatha. Docformerv2: Local features for document understanding. In *Proceedings of the AAAI Conference on Artificial Intelligence*, volume 38, pages 709–718, 2024.
- [4] Minkyung Baek, Frank DiMaio, Ivan Anishchenko, Justas Dauparas, Sergey Ovchinnikov, Gyu Rie Lee, Jue Wang, Qian Cong, Lisa N Kinch, R Dustin Schaeffer, et al. Accurate prediction of protein structures and interactions using a three-track neural network. *Science*, 373(6557):871–876, 2021.
- [5] Jinze Bai, Shuai Bai, Shusheng Yang, Shijie Wang, Sinan Tan, Peng Wang, Junyang Lin, Chang Zhou, and Jingren Zhou. Qwen-vl: A frontier large vision-language model with versatile abilities. *arXiv preprint arXiv:2308.12966*, 2023.
- [6] Yoshua Bengio, Aaron Courville, and Pascal Vincent. Representation learning: A review and new perspectives. *IEEE transactions on pattern analysis and machine intelligence*, 35(8):1798–1828, 2013.
- [7] Zhe Chen, Jiannan Wu, Wenhui Wang, Weijie Su, Guo Chen, Sen Xing, Zhong Muyan, Qinglong Zhang, Xizhou Zhu, Lewei Lu, et al. Internvl: Scaling up vision foundation models and aligning for generic visual-linguistic tasks. *arXiv preprint arXiv:2312.14238*, 2023.
- [8] Zhe Chen, Weiyun Wang, Hao Tian, Shenglong Ye, Zhangwei Gao, Erfei Cui, Wenwen Tong, Kongzhi Hu, Jiapeng Luo, Zheng Ma, et al. How far are we to gpt-4v? closing the gap to commercial multimodal models with open-source suites. *arXiv preprint arXiv:2404.16821*, 2024.
- [9] Cheng Da, Chuwei Luo, Qi Zheng, and Cong Yao. Vision grid transformer for document layout analysis. In *Proceedings of the IEEE/CVF International Conference on Computer Vision*, pages 19462–19472, 2023.
- [10] Alexey Dosovitskiy, Lucas Beyer, Alexander Kolesnikov, Dirk Weissenborn, Xiaohua Zhai, Thomas Unterthiner, Mostafa Dehghani, Matthias Minderer, Georg Heigold, Sylvain Gelly, Jakob Uszkoreit, and Neil Houlsby. An image is worth 16x16 words: Transformers for image recognition at scale. *ArXiv*, abs/2010.11929, 2020.
- [11] Richard Evans, Michael O’Neill, Alexander Pritzel, Natasha Antropova, Andrew Senior, Tim Green, Augustin Žídek, Russ Bates, Sam Blackwell, Jason Yim, Olaf Ronneberger, Sebastian Bodenstein, Michal Zielinski, Alex Bridgland, Anna Potapenko, Andrew Cowie, Kathryn Tunyasuvunakool, Rishabh Jain, Ellen Clancy, Pushmeet Kohli, John Jumper, and Demis Hassabis. Protein complex prediction with alphafold-multimer. *bioRxiv*, 2021. doi: 10.1101/2021.10.04.463034. URL <https://www.biorxiv.org/content/early/2021/10/04/2021.10.04.463034>.
- [12] Jiabang He, Lei Wang, Yi Hu, Ning Liu, Hui Liu, Xing Xu, and Heng Tao Shen. Icl-d3ie: In-context learning with diverse demonstrations updating for document information extraction. In *Proceedings of the IEEE/CVF International Conference on Computer Vision*, pages 19485–19494, 2023.
- [13] Kaiming He, Xinlei Chen, Saining Xie, Yanghao Li, Piotr Dollár, and Ross Girshick. Masked autoencoders are scalable vision learners. In *Proceedings of the IEEE/CVF conference on computer vision and pattern recognition*, pages 16000–16009, 2022.
- [14] Xinyi He, Mengyu Zhou, Xinrun Xu, Xiaojun Ma, Rui Ding, Lun Du, Yan Gao, Ran Jia, Xu Chen, Shi Han, et al. Text2analysis: A benchmark of table question answering with advanced data analysis and unclear queries. *arXiv preprint arXiv:2312.13671*, 2023.
- [15] Wenyi Hong, Weihan Wang, Qingsong Lv, Jiazheng Xu, Wenmeng Yu, Junhui Ji, Yan Wang, Zihan Wang, Yuxiao Dong, Ming Ding, et al. Cogagent: A visual language model for gui agents. *arXiv preprint arXiv:2312.08914*, 2023.
- [16] Anwen Hu, Haiyang Xu, Jiabo Ye, Ming Yan, Liang Zhang, Bo Zhang, Chen Li, Ji Zhang, Qin Jin, Fei Huang, et al. mplug-docowl 1.5: Unified structure learning for ocr-free document understanding. *arXiv preprint arXiv:2403.12895*, 2024.
- [17] Yupan Huang, Tengchao Lv, Lei Cui, Yutong Lu, and Furu Wei. Layoutlmv3: Pre-training for document ai with unified text and image masking. In *Proceedings of the 30th ACM International Conference on Multimedia*, pages 4083–4091, 2022.

- [18] Glenn Jocher, Ayush Chaurasia, and Jing Qiu. Ultralytics YOLO, January 2023. URL <https://github.com/ultralytics/ultralytics>.
- [19] John Jumper, Richard Evans, Alexander Pritzel, Tim Green, Michael Figurnov, Olaf Ronneberger, Kathryn Tunyasuvunakool, Russ Bates, Augustin Žídek, Anna Potapenko, Alex Bridgland, Clemens Meyer, Simon A A Kohl, Andrew J Ballard, Andrew Cowie, Bernardino Romera-Paredes, Stanislav Nikolov, Rishabh Jain, Jonas Adler, Trevor Back, Stig Petersen, David Reiman, Ellen Clancy, Michal Zielinski, Martin Steinegger, Michalina Pacholska, Tamas Berghammer, Sebastian Bodenstein, David Silver, Oriol Vinyals, Andrew W Senior, Koray Kavukcuoglu, Pushmeet Kohli, and Demis Hassabis. Highly accurate protein structure prediction with AlphaFold. *Nature*, 596(7873):583–589, 2021. doi: 10.1038/s41586-021-03819-2.
- [20] Kenton Lee, Mandar Joshi, Iulia Raluca Turc, Hexiang Hu, Fangyu Liu, Julian Martin Eisenschlos, Urvashi Khandelwal, Peter Shaw, Ming-Wei Chang, and Kristina Toutanova. Pix2struct: Screenshot parsing as pretraining for visual language understanding. In *International Conference on Machine Learning*, pages 18893–18912. PMLR, 2023.
- [21] Lei Li, Yuqi Wang, Runxin Xu, Peiyi Wang, Xiachong Feng, Lingpeng Kong, and Qi Liu. Multimodal arxiv: A dataset for improving scientific comprehension of large vision-language models. *arXiv preprint arXiv:2403.00231*, 2024.
- [22] Minghao Li, Yiheng Xu, Lei Cui, Shaohan Huang, Furu Wei, Zhoujun Li, and Ming Zhou. Docbank: A benchmark dataset for document layout analysis. *arXiv preprint arXiv:2006.01038*, 2020.
- [23] Zhang Li, Biao Yang, Qiang Liu, Zhiyin Ma, Shuo Zhang, Jingxu Yang, Yabo Sun, Yuliang Liu, and Xiang Bai. Monkey: Image resolution and text label are important things for large multi-modal models. *arXiv preprint arXiv:2311.06607*, 2023.
- [24] Bin Lin, Zhenyu Tang, Yang Ye, Jiaxi Cui, Bin Zhu, Peng Jin, Junwu Zhang, Munan Ning, and Li Yuan. Moe-llava: Mixture of experts for large vision-language models. *arXiv preprint arXiv:2401.15947*, 2024.
- [25] Chenglong Liu, Haoran Wei, Jinyue Chen, Lingyu Kong, Zheng Ge, Zining Zhu, Liang Zhao, Jianjian Sun, Chunrui Han, and Xiangyu Zhang. Focus anywhere for fine-grained multi-page document understanding. *arXiv preprint arXiv:2405.14295*, 2024.
- [26] Yuliang Liu, Biao Yang, Qiang Liu, Zhang Li, Zhiyin Ma, Shuo Zhang, and Xiang Bai. Textmonkey: An ocr-free large multimodal model for understanding document. *arXiv preprint arXiv:2403.04473*, 2024.
- [27] Zhaoyang Liu, Zeqiang Lai, Zhangwei Gao, Erfei Cui, Zhiheng Li, Xizhou Zhu, Lewei Lu, Qifeng Chen, Yu Qiao, Jifeng Dai, et al. Controlllm: Augment language models with tools by searching on graphs. *arXiv preprint arXiv:2310.17796*, 2023.
- [28] Ilya Loshchilov and Frank Hutter. Decoupled weight decay regularization. *arXiv preprint arXiv:1711.05101*, 2017.
- [29] Xudong Lu, Qi Liu, Yuhui Xu, Aojun Zhou, Siyuan Huang, Bo Zhang, Junchi Yan, and Hongsheng Li. Not all experts are equal: Efficient expert pruning and skipping for mixture-of-experts large language models. *arXiv preprint arXiv:2402.14800*, 2024.
- [30] Chuwei Luo, Yufan Shen, Zhaoqing Zhu, Qi Zheng, Zhi Yu, and Cong Yao. Layoutllm: Layout instruction tuning with large language models for document understanding. *arXiv preprint arXiv:2404.05225*, 2024.
- [31] Tengchao Lv, Yupan Huang, Jingye Chen, Lei Cui, Shuming Ma, Yaoyao Chang, Shaohan Huang, Wenhui Wang, Li Dong, Weiyao Luo, et al. Kosmos-2.5: A multimodal literate model. *arXiv preprint arXiv:2309.11419*, 2023.
- [32] Minesh Mathew, Dimosthenis Karatzas, and CV Jawahar. Docvqa: A dataset for vqa on document images. In *Proceedings of the IEEE/CVF winter conference on applications of computer vision*, pages 2200–2209, 2021.
- [33] OpenAI. Gpt-4v(ision) system card. <https://openai.com/contributions/gpt-4v>, 2023.
- [34] Birgit Pfitzmann, Christoph Auer, Michele Dolfi, Ahmed S Nassar, and Peter Staar. Doclaynet: a large human-annotated dataset for document-layout segmentation. In *Proceedings of the 28th ACM SIGKDD Conference on Knowledge Discovery and Data Mining*, pages 3743–3751, 2022.
- [35] Machel Reid, Nikolay Savinov, Denis Teplyashin, Dmitry Lepikhin, Timothy Lillicrap, Jean-baptiste Alayrac, Radu Soricut, Angeliki Lazaridou, Orhan Firat, Julian Schrittweiser, et al. Gemini 1.5: Unlocking multimodal understanding across millions of tokens of context. *arXiv preprint arXiv:2403.05530*, 2024.

- [36] Quan Sun, Qiying Yu, Yufeng Cui, Fan Zhang, Xiaosong Zhang, Yueze Wang, Hongcheng Gao, Jingjing Liu, Tiejun Huang, and Xinlong Wang. Generative pretraining in multimodality. *arXiv preprint arXiv:2307.05222*, 2023.
- [37] Zineng Tang, Ziyi Yang, Guoxin Wang, Yuwei Fang, Yang Liu, Chenguang Zhu, Michael Zeng, Cha Zhang, and Mohit Bansal. Unifying vision, text, and layout for universal document processing. In *Proceedings of the IEEE/CVF Conference on Computer Vision and Pattern Recognition*, pages 19254–19264, 2023.
- [38] Gemini Team, Rohan Anil, Sebastian Borgeaud, Yonghui Wu, Jean-Baptiste Alayrac, Jiahui Yu, Radu Soricut, Johan Schalkwyk, Andrew M Dai, Anja Hauth, et al. Gemini: a family of highly capable multimodal models. *arXiv preprint arXiv:2312.11805*, 2023.
- [39] Changyao Tian, Xizhou Zhu, Yuwen Xiong, Weiyun Wang, Zhe Chen, Wenhai Wang, Yuntao Chen, Lewei Lu, Tong Lu, Jie Zhou, et al. Mm-interleaved: Interleaved image-text generative modeling via multi-modal feature synchronizer. *arXiv preprint arXiv:2401.10208*, 2024.
- [40] Jordy Van Landeghem, Rubén Tito, Łukasz Borchmann, Michał Pietruszka, Paweł Joziāk, Rafal Powalski, Dawid Jurkiewicz, Mickaël Coustaty, Bertrand Anckaert, Ernest Valveny, et al. Document understanding dataset and evaluation (dude). In *Proceedings of the IEEE/CVF International Conference on Computer Vision*, pages 19528–19540, 2023.
- [41] Ashish Vaswani, Noam M. Shazeer, Niki Parmar, Jakob Uszkoreit, Llion Jones, Aidan N. Gomez, Łukasz Kaiser, and Illia Polosukhin. Attention is all you need. In *Neural Information Processing Systems*, 2017. URL <https://api.semanticscholar.org/CorpusID:13756489>.
- [42] Bin Wang, Zhuangcheng Gu, Chao Xu, Bo Zhang, Botian Shi, and Conghui He. Unimernet: A universal network for real-world mathematical expression recognition. *arXiv preprint arXiv:2404.15254*, 2024.
- [43] Dongsheng Wang, Natraj Raman, Mathieu Sibue, Zhiqiang Ma, Petr Babkin, Simerjot Kaur, Yulong Pei, Armeneh Nourbakhsh, and Xiaomo Liu. Docllm: A layout-aware generative language model for multimodal document understanding. *arXiv preprint arXiv:2401.00908*, 2023.
- [44] Weihua Wang, Qingsong Lv, Wenmeng Yu, Wenyi Hong, Ji Qi, Yan Wang, Junhui Ji, Zhuoyi Yang, Lei Zhao, Xixuan Song, et al. Cogylm: Visual expert for pretrained language models. *arXiv preprint arXiv:2311.03079*, 2023.
- [45] Weiyun Wang, Yiming Ren, Haowen Luo, Tiantong Li, Chenxiang Yan, Zhe Chen, Wenhai Wang, Qingyun Li, Lewei Lu, Xizhou Zhu, et al. The all-seeing project v2: Towards general relation comprehension of the open world. *arXiv preprint arXiv:2402.19474*, 2024.
- [46] Yi Wang, Kunchang Li, Xinhao Li, Jiashuo Yu, Yinan He, Guo Chen, Baoqi Pei, Rongkun Zheng, Jilan Xu, Zun Wang, et al. Internvideo2: Scaling video foundation models for multimodal video understanding. *arXiv preprint arXiv:2403.15377*, 2024.
- [47] Zilong Wang, Yichao Zhou, Wei Wei, Chen-Yu Lee, and Sandeep Tata. Vrdu: A benchmark for visually-rich document understanding. In *Proceedings of the 29th ACM SIGKDD Conference on Knowledge Discovery and Data Mining*, pages 5184–5193, 2023.
- [48] Shengqiong Wu, Hao Fei, Leigang Qu, Wei Ji, and Tat-Seng Chua. Next-gpt: Any-to-any multimodal llm. *arXiv preprint arXiv:2309.05519*, 2023.
- [49] Renqiu Xia, Bo Zhang, Haoyang Peng, Ning Liao, Peng Ye, Botian Shi, Junchi Yan, and Yu Qiao. Structchart: Perception, structuring, reasoning for visual chart understanding. *arXiv preprint arXiv:2309.11268*, 2023.
- [50] Renqiu Xia, Bo Zhang, Hancheng Ye, Xiangchao Yan, Qi Liu, Hongbin Zhou, Zijun Chen, Min Dou, Botian Shi, Junchi Yan, et al. Chartx & chartvlm: A versatile benchmark and foundation model for complicated chart reasoning. *arXiv preprint arXiv:2402.12185*, 2024.
- [51] Cong Yao. Docxchain: A powerful open-source toolchain for document parsing and beyond. *arXiv preprint arXiv:2310.12430*, 2023.
- [52] Jiabo Ye, Anwen Hu, Haiyang Xu, Qinghao Ye, Ming Yan, Yuhao Dan, Chenlin Zhao, Guohai Xu, Chenliang Li, Junfeng Tian, et al. mplug-docowl: Modularized multimodal large language model for document understanding. *arXiv preprint arXiv:2307.02499*, 2023.
- [53] Shilong Zhang, Peize Sun, Shoufa Chen, Min Xiao, Wenqi Shao, Wenwei Zhang, Kai Chen, and Ping Luo. Gpt4roi: Instruction tuning large language model on region-of-interest. *arXiv preprint arXiv:2307.03601*, 2023.

- [54] Xu Zhong, Jianbin Tang, and Antonio Jimeno Yepes. Publaynet: largest dataset ever for document layout analysis. In *2019 International conference on document analysis and recognition (ICDAR)*, pages 1015–1022. IEEE, 2019.
- [55] Zhanpeng Zhou, Zijun Chen, Yilan Chen, Bo Zhang, and Junchi Yan. Cross-task linearity emerges in the pretraining-finetuning paradigm. *arXiv preprint arXiv:2402.03660*, 2024.
- [56] Deyao Zhu, Jun Chen, Xiaoqian Shen, Xiang Li, and Mohamed Elhoseiny. Minigpt-4: Enhancing vision-language understanding with advanced large language models. *arXiv preprint arXiv:2304.10592*, 2023.

A Overview of Appendix

We provide more information on our benchmark and further experiment details from the following aspects:

- Sec. **B**: Limitations and Dataset Accessibility.
 - Sec. **B.1**: Limitations.
 - Sec. **B.2**: Dataset Accessibility.
- Sec. **C**: Annotation Explanations.
- Sec. **D**: More Statistical Distributions of DocGenome.
- Sec. **E**: Details of Quality Assurance.
- Sec. **F**: Prompt Design for GPT-acc.
- Sec. **G**: Annotation Examples in DocGenome.
- Sec. **H**: Task Examples in DocGenome-test.

B Limitations and Dataset Accessibility

B.1 Limitations

The purpose of our DocGenome is to build a comprehensive scientific document dataset, promoting the development of intelligent document processing and effective evaluation of MLLMs in document understanding tasks. Although our DocGenome provides annotations for 6 categories of entity relationships, exploring the impact of these entity relationship annotations on large models' understanding of scientific documents is highly meaningful. For future works, we will explore the role of the entity relationships in understanding scientific documents.

B.2 Dataset Accessibility

Dataset Documentation: We have documented our dataset and its intended uses, as required. The website of our dataset is available at the following link: <https://github.com/UniModal4Reasoning/DocGenome>, which includes metadata, format details, and visualizations. Besides, the download link for the dataset is: https://drive.google.com/drive/folders/10IhnuQdIjuSSDc_QL2nP4NwugVDgtItD?usp=sharing.

Dataset Statistics and Analyses: We have conducted extensive data statistics and analyses, along with thorough quality checks including DocGenome-train and DocGenome-test datasets, which are presented in Sec. 3.2 and Sec. 4.2.

Long-term Preservation: To ensure the long-term preservation of the DocGenome dataset, we have uploaded it to Google Drive^{\$}. This ensures continuous accessibility to the dataset for an extended duration. Furthermore, we will routinely back up the data and monitor its availability to maintain continued accessibility.

Terms of Use and License: We have chosen the CC BY 4.0 license for our dataset, as required. This information is included in our paper submission and will also be clearly stated on our dataset website.

A Persistent Dereferenceable Identifier: We have obtained a DOI for our dataset, referred to as [10.5281/zenodo.11488587](https://doi.org/10.5281/zenodo.11488587). This persistent dereferenceable identifier ensures long-term accessibility and citability of the dataset.

Discussion of Personally Identifiable Information. All the scientific documents in our DocGenome are sourced from the arXiv open-access community, where papers are released under the CC license. Besides, the arXiv community ensures that papers uploaded by authors adhere to legal and ethical guidelines, including the protection of personal information and the avoidance of offensive material. Thus, we can confirm that our DocGenome does not contain personally identifiable information or offensive content.

^{\$}The download link for the dataset is available at: https://drive.google.com/drive/folders/10IhnuQdIjuSSDc_QL2nP4NwugVDgtItD?usp=sharing.

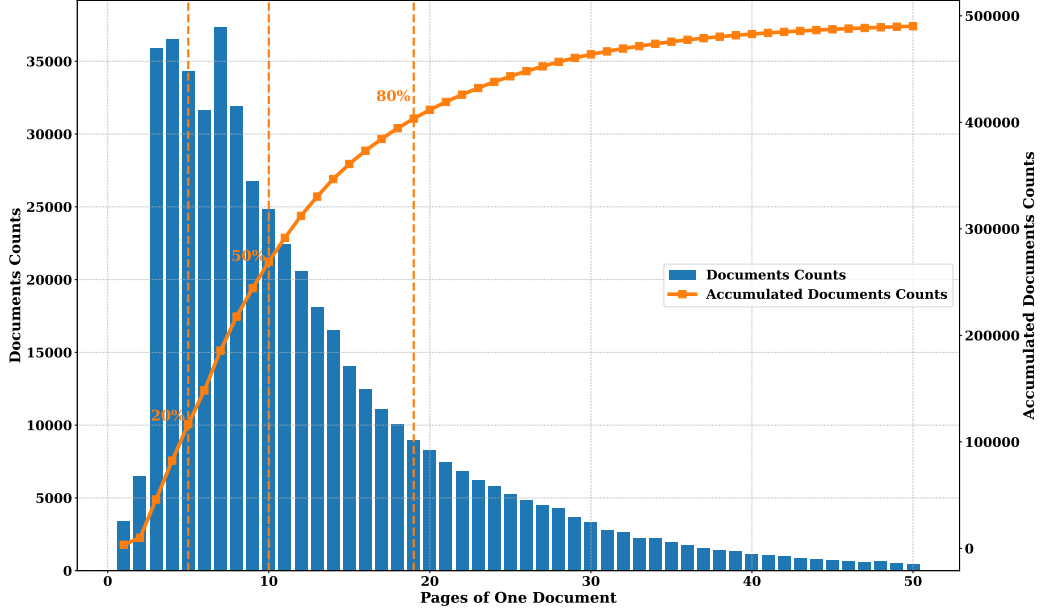


Figure A.1: Page distribution of DocGenome. 20% of documents are five pages or fewer, 50% are ten pages or fewer, and 80% are nineteen pages or fewer.

Table A.1: Category descriptions of the layout annotation performed by our DocParser. Note that we do not use the “others” category and the “reference” category, and their indices are 6 and 11, respectively.

Index	Category	Notes
0	Algorithm	
1	Caption	Titles of Images, Tables, and Algorithms
2	Equation	
3	Figure	
4	Footnote	
5	List	
7	Table	
8	Text	
9	Text-EQ	Text block with inline equations
10	Title	Section titles
12	PaperTitle	
13	Code	
14	Abstract	

C Annotation Explanations

We provide the annotation details of DocGenome in Table A.1, where the index number in the annotation corresponds to the category index in the attribute list.

D More Statistical Distributions of DocGenome

In addition to the statistical distribution described in Sec. 3, we provide more statistical distributions in this section. As shown in Fig. A.2, the sample counts of all secondary disciplines are summarized and marked with different colors, from which it can be observed that the inter-discipline and intra-discipline distributions are both diverse, with Physics, Computer Science, and Mathematics papers occupying the major components of DocGenome.

[‡]The version of the online API we used for evaluation: <https://mathpix.com/equation-to-latex>.

[§]Online API we used for evaluation: <https://mathpix.com/table-to-latex>.

We also present the page distribution of DocGenome in Fig. A.1, which indicates the diversity of paper length in DocGenome. Specifically, 50% papers in DocGenome have nearly or fewer than 10 pages, with 80% papers having fewer than 19 pages.

E Details of Quality Assurance for QA Data

The QA Generation Details. We provide a general prompt template for QA pair generation in Fig. A.3. The discipline-specific guidance is imposed to generate the corresponding ground-truth labels to achieve diversity and relevance.

The Quality Checking Details. During independent verification by professional faculty members, each judgment was assigned with a confidence value ranging from 0 to 3. The confidence criterion is designed as follows:

Confidence 3: The reviewer is confident that the QA pair is accurate and relevant to the provided paper.

Confidence 2: The reviewer thinks the QA pair is mostly accurate and relevant to the provided paper but is unsure whether it is absolutely correct.

Confidence 1: The reviewer has no idea about the correctness or relevance of the QA pair to the provided paper.

Confidence 0: The reviewer is confident that the QA pair is wrong or irrelevant to the provided paper.

During the cross-verification, the confidence values of the two professional faculty reviewers were compared with the automatically-annotated correctness. The QA pairs with inconsistent results were re-analyzed by the two reviewers and updated to a precise version with consistent confidence.

F Prompt Design for GPT-acc

We adopt GPT-acc as the evaluation metric for the QA tasks. The complete prompts are concluded in Fig. A.4.

G Examples in Document-level Annotation from DocGenome

We present one example in DocGenome in Figs. A.5, A.6, and A.7 to visualize the annotations of each page in a whole document [41]. The blocks marked with different colors refer to different attributes of component units and the arrows with different colors denote different relations between units.

H Examples of Tasks in DocGenome-test

We provide visual demonstrations in Fig. A.8 for all 7 tasks in DocGenome-test, including document classification, visual grounding, open-ended single-page and multi-page QA tasks, document layout detection, Equation-to-L^AT_EX transformation, and Table-to-L^AT_EX transformation.

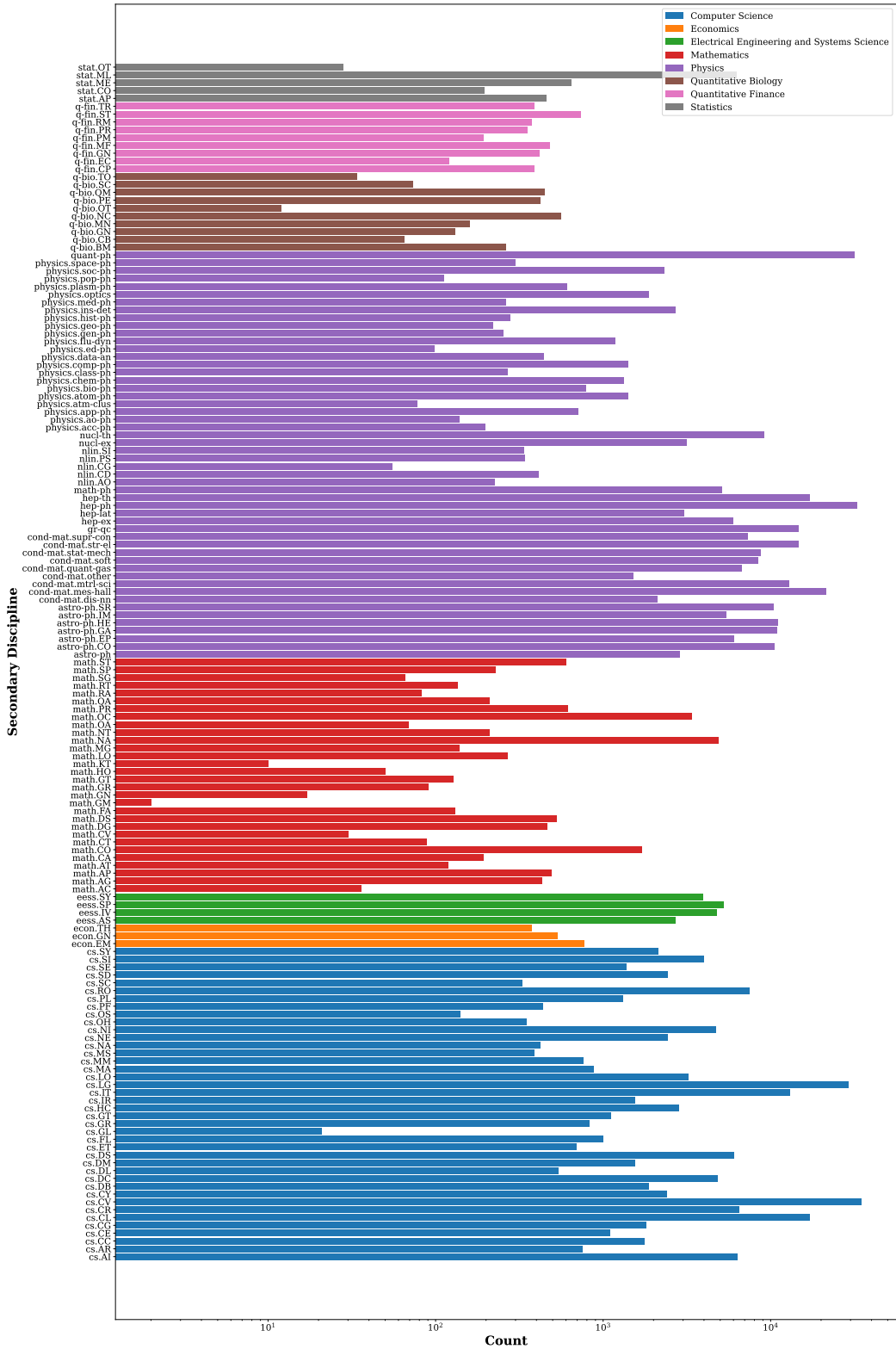


Figure A.2: Distribution of secondary disciplines in our DocGenome. The count on the x-axis represents the number of documents, and documents from the same primary discipline are marked with the same color.

 **QA Generation Template**

Assume you are an expert in the analysis of arxiv papers. Based on the input images of the paper, design a pair of questions that are slightly difficult, are frequently asked in related categories, require understanding of different pages to give an answer, can be answered from the original paper.
 Each answer should not contain any hints, explanations, or notes, etc.
 Make sure your answers are accurate. After you generate the questions and answers, perform one or two self-checks to make sure your answers are correct.
 Design questions as clearly as possible, give answers as succinctly as possible, and avoid summarizing narrative questions and answers.

The questions should be in the form of a question-answer pair.
 Make sure the answer to the question is taken directly from the original text, not from your summary and make sure answers are as short and direct as possible.

Here are some simple examples:

1. Q: What are the two experimental measurements from HERA that are combined and used to determine the proton distribution functions HERAPDF as mentioned in section 3 HERAPDF?
 A: H1 and ZEUS
2. Q: What are the two main types of deep inelastic scattering experiments discussed in the paper?
 A: Inclusive and semi-inclusive
3. Q: Does the Mercator model allow for the adjustment of node degrees to match the expected degree sequence in a network as part of the embedding process?
 A: Yes
4. Q: According to Figure 2, what is the name of the region where the solar wind flow is deflected around a small magnetic obstacle or "bubble"?
 A: Narrow barrier region
5. Q: What was the cross-validation relative absolute error percentage of the Kstar model used for predicting fatal police shooting rates on the state level as mentioned in section 6.1?
 A: 28.53%

Please follow this format and give two pairs of answers to the questions.

Figure A.3: Template prompts using GPT-4V [33] for document QA pair generation.

 **GPT-acc for DocVQA**

Examples:

```
{
  "query": "<question> What was the incremental increase in revenue from 2020 to 2021? <groundtruth answer> 5 million $. <answer> 20\n</s>",
  "answer": "False"
},
{
  "query": "<question> What percentage of government spending was allocated to infrastructure in 2020? <groundtruth answer> 10% <answer> 14-4=10\n</s>",
  "answer": "True"
},
{
  "query": "<question> What is the total production of Wind Energy in the four months from January to April 2021? <groundtruth answer> 2300 MW <answer> The total production of Wind Energy in the four months from January to April 2021 is 2450 MW.",
  "answer": "False"
},
{
  "query": "<question> What is the value of baseline distance L for the DUNE analysis mentioned in Table I? <groundtruth answer> 1300km <answer> The value of baseline distance L for the DUNE analysis mentioned in Table I is 1300km.",
  "answer": "True"
},
{
  "query": "<question> According to the caption of Figure 5, what is the fixed value of M_N1 used to predict the relic density as a function of m_n? <groundtruth answer> 200 GeV <answer> The fixed value of M_N1 used to predict the relic density as a function of m_n is 200 GeV.",
  "answer": "True"
}
```

Instruction:

Given multiple question-answer pairs and the corresponding predictions, evaluate the correctness of predictions.
 The output should be only "True" or "False"

Input:

```
f```
<question> {question} <groundtruth answer> {answer_gt} <answer> {answer_pred}
```
```

Figure A.4: Detailed prompts in GPT-acc metric for document QA tasks.

# Visualization of Annotations in DocGenome

Page 1 of 10



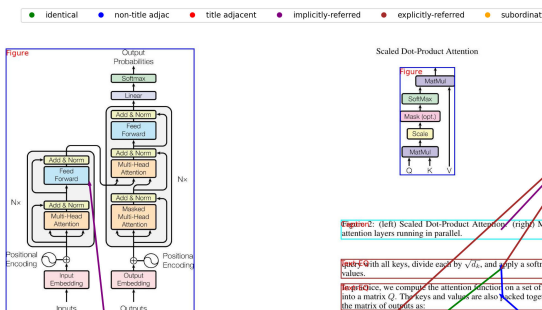
## Title: Introduction

Recurrent neural networks, long short-term memory [13] and gated recurrent [2] neural networks in particular, have been firmly established as state-of-the-art approaches in sequence modeling and “Footnote contribution: Listing order is random. Jakob proposed replacing RNNs with self-attention and started the effort to evaluate this idea. Ashish, Neel, designed and implemented the first Transformer models and have been the primary contributors to the subsequent work. Lukasz, Aidan, and Illia designed and implemented multi-head attention and the parameter-free position representation and became the other person involved in nearly every detail. Niki designed, implemented, tuned and evaluated countless model variants in our original codebase and tensor library. Llion and Jakob were the main implementors of the PyTorch implementation of the Transformer and efficient inference and visualizations. Lukasz and Aidan spent countless long days debugging parts of and implementing tensorflow, greatly improving results and massively accelerating our research.

<sup>\*</sup>Work performed while at Google Brain.

<sup>†</sup>Work performed while at Google Research.

31st Conference on Neural Information Processing Systems (NIPS 2017), Long Beach, CA, USA.



**Encoder:** The encoder is composed of a stack of  $N = 6$  identical layers. Each layer has two sub-layers. The first is a multi-head self-attention mechanism, and the second is a simple, position-wise fully connected feed-forward network. We employ a residual connection [11] around each of the two sub-layers, followed by a layer normalization [1]. That is, the output of each layer is  $\text{LayerNorm}(\text{Sublayer}_2(\text{Sublayer}_1(x)))$ , where  $\text{Sublayer}_1(x)$  is the attention implemented by the sub-layer itself. To facilitate these residual connections,  $N$  sub-layers in the model, as well as the embedding layers, produce outputs of dimension  $d_{\text{model}} = 512$ .

**Decoder:** The decoder is also composed of a stack of  $N = 6$  identical layers. In addition to the two sub-layers of the encoder, the decoder has one additional sub-layer, which performs cross-attention over the output of the encoder stack. Similar to the encoder, the residual connection around each of the sub-layers follows a layer normalization. We also modify the self-attention layer in the decoder to prevent gradients from attending to subsequent positions. This masking is done with care so that our embeddings are offset by one position. Thus the predictions for position  $i$  depend only on the known numbers at positions less than  $i$ .

## 3.2. Attention

**Naive attention** can be described as mapping a query and a set of key-value pairs to an output, where the query, keys, values, and all being all vectors. The output is computed as a weighted sum of the values, where the weight assigned to each value is computed by a compatibility function of the query with its corresponding key.

### 3.2.1. Scaled Dot-Product Attention

While our particular attention “Scaled Dot-Product Attention” (Figure 2). The input consists of queries and keys of dimension  $d_q$ , and values of dimension  $d_v$ . We compute the dot products of the

Page 2 of 10

Input reduction problems such as language modeling and machine translation [34, 35]. Numerous efforts have since worked to push the boundaries of recurrent language models and encoder-decoder architectures [36, 24, 15].

**Recurrent models** typically factor computation along the symbol positions of the input and output sequences. Aligning the positions to steps in computation time, they generate a sequence of hidden states  $h_t$ , as a function of the previous hidden state  $h_{t-1}$  and the input for position  $t$ . This inherently requires computation to be aligned with the sequence length. As sequences grow longer and longer, sequence lengths, as memory constraints limit the amount of computation that can be shared across examples. Recent work has achieved significant improvements in computational efficiency through factorization tricks [2] and conditional computation [32]. These improvements in performance in case of the latter. The fundamental constraint of sequential computation, however,

**Attention mechanisms** have become an integral part of compelling sequence modeling and transduction models in various tasks, due to their ability of dependencies without regard to their distance in the input or output sequence [23]. In a host of few cases [2], however, such attention mechanisms are used in conjunction with a recurrent network.

**Today** we propose the Transformer, a model architecture eschewing recurrence and instead relying entirely on an attention mechanism to draw global dependencies between input and output. The Transformer allows for significantly more parallelization and can reach a new state of the art in translation quality after being trained for as little as twelve hours on eight P100 GPUs.

## 3.3. Background

The goal of reducing sequential computation also forms the foundation of the Extended Neural GPU [16], ByteNet [18] and Transformer [36], all of which have used neural networks as building blocks to process sequences. While these models represent a significant improvement over these models, the number of operations required to move signals from two arbitrary input or output position grows in the distance between positions, linearly for ByteNet and logarithmically for Transformer. This makes it more difficult to parallelize dependencies between distant positions [18]. At the same time, this is reduced to a constant number of operations per position at the cost of reduced effective resolution due to avoiding attention-weighted positions, and effect we counteract with Multi-Head Attention as described below.

**Self-attention**, sometimes called intra-attention, is an attention mechanism relating different positions of a single sequence in order to handle a representation’s compositionality. Self-attention has been used successfully in a variety of tasks, including document summarization, image captioning, visual question answering and language tasks like sentence representations [4, 7, 12, 27].

**Bidirectional memory networks** are based on recurrent attention mechanism instead of sequence-aligned recurrence and have been shown to perform well on simple language question answering and language modeling tasks [23].

**Very recently**, we note that, however, the Transformer is the first transduction model relying entirely on self-attention to compute representations of its input and output without using sequence-aligned RNNs or convolution. In the following sections, we will describe the Transformer, motivate self-attention and discuss its advantages over models such as [17, 18] and [9].

## 3.4. Encoder and Decoder Stacks

**Encoder** and **decoder** stacks have an encoder-decoder structure [26, 10]. Here, the encoder maps an input sequence of symbol representations  $(x_1, \dots, x_n)$  to a sequence of continuous dense representations  $z = (z_1, \dots, z_n)$ . Given  $z$ , the decoder then generates an output sequence  $y = (y_1, \dots, y_m)$  via one-to-many decoding, as shown in Figure 3. At each step  $t$ , the decoder [19] consumes the previously generated symbols as additional input when generating the next.

**The Transformer** follows this overall architecture using stacked self-attention and point-wise, fully connected layers for both the encoder and decoder, shown in the left and right halves of Figure 1 respectively.

## 3.5. Encoder and Decoder Stacks

**Encoder** and **decoder** stacks have an encoder-decoder structure [26, 10].

Here, the encoder maps an input sequence of symbol representations  $(x_1, \dots, x_n)$  to a sequence of continuous dense representations  $z = (z_1, \dots, z_n)$ . Given  $z$ , the decoder then generates an output sequence  $y = (y_1, \dots, y_m)$  via one-to-many decoding, as shown in Figure 3. At each step  $t$ , the decoder [19] consumes the previously generated symbols as additional input when generating the next.

**The Transformer** follows this overall architecture using stacked self-attention and point-wise, fully connected layers for both the encoder and decoder, shown in the left and right halves of Figure 1 respectively.

## 3.6. Encoder and Decoder Stacks

**Encoder** and **decoder** stacks have an encoder-decoder structure [26, 10].

Here, the encoder maps an input sequence of symbol representations  $(x_1, \dots, x_n)$  to a sequence of continuous dense representations  $z = (z_1, \dots, z_n)$ . Given  $z$ , the decoder then generates an output sequence  $y = (y_1, \dots, y_m)$  via one-to-many decoding, as shown in Figure 3. At each step  $t$ , the decoder [19] consumes the previously generated symbols as additional input when generating the next.

**The Transformer** follows this overall architecture using stacked self-attention and point-wise, fully connected layers for both the encoder and decoder, shown in the left and right halves of Figure 1 respectively.

## 3.7. Encoder and Decoder Stacks

**Encoder** and **decoder** stacks have an encoder-decoder structure [26, 10].

Here, the encoder maps an input sequence of symbol representations  $(x_1, \dots, x_n)$  to a sequence of continuous dense representations  $z = (z_1, \dots, z_n)$ . Given  $z$ , the decoder then generates an output sequence  $y = (y_1, \dots, y_m)$  via one-to-many decoding, as shown in Figure 3. At each step  $t$ , the decoder [19] consumes the previously generated symbols as additional input when generating the next.

**The Transformer** follows this overall architecture using stacked self-attention and point-wise, fully connected layers for both the encoder and decoder, shown in the left and right halves of Figure 1 respectively.

## 3.8. Encoder and Decoder Stacks

**Encoder** and **decoder** stacks have an encoder-decoder structure [26, 10].

Here, the encoder maps an input sequence of symbol representations  $(x_1, \dots, x_n)$  to a sequence of continuous dense representations  $z = (z_1, \dots, z_n)$ . Given  $z$ , the decoder then generates an output sequence  $y = (y_1, \dots, y_m)$  via one-to-many decoding, as shown in Figure 3. At each step  $t$ , the decoder [19] consumes the previously generated symbols as additional input when generating the next.

**The Transformer** follows this overall architecture using stacked self-attention and point-wise, fully connected layers for both the encoder and decoder, shown in the left and right halves of Figure 1 respectively.

## 3.9. Encoder and Decoder Stacks

**Encoder** and **decoder** stacks have an encoder-decoder structure [26, 10].

Here, the encoder maps an input sequence of symbol representations  $(x_1, \dots, x_n)$  to a sequence of continuous dense representations  $z = (z_1, \dots, z_n)$ . Given  $z$ , the decoder then generates an output sequence  $y = (y_1, \dots, y_m)$  via one-to-many decoding, as shown in Figure 3. At each step  $t$ , the decoder [19] consumes the previously generated symbols as additional input when generating the next.

**The Transformer** follows this overall architecture using stacked self-attention and point-wise, fully connected layers for both the encoder and decoder, shown in the left and right halves of Figure 1 respectively.

## 3.10. Encoder and Decoder Stacks

**Encoder** and **decoder** stacks have an encoder-decoder structure [26, 10].

Here, the encoder maps an input sequence of symbol representations  $(x_1, \dots, x_n)$  to a sequence of continuous dense representations  $z = (z_1, \dots, z_n)$ . Given  $z$ , the decoder then generates an output sequence  $y = (y_1, \dots, y_m)$  via one-to-many decoding, as shown in Figure 3. At each step  $t$ , the decoder [19] consumes the previously generated symbols as additional input when generating the next.

**The Transformer** follows this overall architecture using stacked self-attention and point-wise, fully connected layers for both the encoder and decoder, shown in the left and right halves of Figure 1 respectively.

## 3.11. Encoder and Decoder Stacks

**Encoder** and **decoder** stacks have an encoder-decoder structure [26, 10].

Here, the encoder maps an input sequence of symbol representations  $(x_1, \dots, x_n)$  to a sequence of continuous dense representations  $z = (z_1, \dots, z_n)$ . Given  $z$ , the decoder then generates an output sequence  $y = (y_1, \dots, y_m)$  via one-to-many decoding, as shown in Figure 3. At each step  $t$ , the decoder [19] consumes the previously generated symbols as additional input when generating the next.

**The Transformer** follows this overall architecture using stacked self-attention and point-wise, fully connected layers for both the encoder and decoder, shown in the left and right halves of Figure 1 respectively.

## 3.12. Encoder and Decoder Stacks

**Encoder** and **decoder** stacks have an encoder-decoder structure [26, 10].

Here, the encoder maps an input sequence of symbol representations  $(x_1, \dots, x_n)$  to a sequence of continuous dense representations  $z = (z_1, \dots, z_n)$ . Given  $z$ , the decoder then generates an output sequence  $y = (y_1, \dots, y_m)$  via one-to-many decoding, as shown in Figure 3. At each step  $t$ , the decoder [19] consumes the previously generated symbols as additional input when generating the next.

**The Transformer** follows this overall architecture using stacked self-attention and point-wise, fully connected layers for both the encoder and decoder, shown in the left and right halves of Figure 1 respectively.

## 3.13. Encoder and Decoder Stacks

**Encoder** and **decoder** stacks have an encoder-decoder structure [26, 10].

Here, the encoder maps an input sequence of symbol representations  $(x_1, \dots, x_n)$  to a sequence of continuous dense representations  $z = (z_1, \dots, z_n)$ . Given  $z$ , the decoder then generates an output sequence  $y = (y_1, \dots, y_m)$  via one-to-many decoding, as shown in Figure 3. At each step  $t$ , the decoder [19] consumes the previously generated symbols as additional input when generating the next.

**The Transformer** follows this overall architecture using stacked self-attention and point-wise, fully connected layers for both the encoder and decoder, shown in the left and right halves of Figure 1 respectively.

## 3.14. Encoder and Decoder Stacks

**Encoder** and **decoder** stacks have an encoder-decoder structure [26, 10].

Here, the encoder maps an input sequence of symbol representations  $(x_1, \dots, x_n)$  to a sequence of continuous dense representations  $z = (z_1, \dots, z_n)$ . Given  $z$ , the decoder then generates an output sequence  $y = (y_1, \dots, y_m)$  via one-to-many decoding, as shown in Figure 3. At each step  $t$ , the decoder [19] consumes the previously generated symbols as additional input when generating the next.

**The Transformer** follows this overall architecture using stacked self-attention and point-wise, fully connected layers for both the encoder and decoder, shown in the left and right halves of Figure 1 respectively.

## 3.15. Encoder and Decoder Stacks

**Encoder** and **decoder** stacks have an encoder-decoder structure [26, 10].

Here, the encoder maps an input sequence of symbol representations  $(x_1, \dots, x_n)$  to a sequence of continuous dense representations  $z = (z_1, \dots, z_n)$ . Given  $z$ , the decoder then generates an output sequence  $y = (y_1, \dots, y_m)$  via one-to-many decoding, as shown in Figure 3. At each step  $t$ , the decoder [19] consumes the previously generated symbols as additional input when generating the next.

**The Transformer** follows this overall architecture using stacked self-attention and point-wise, fully connected layers for both the encoder and decoder, shown in the left and right halves of Figure 1 respectively.

## 3.16. Encoder and Decoder Stacks

**Encoder** and **decoder** stacks have an encoder-decoder structure [26, 10].

Here, the encoder maps an input sequence of symbol representations  $(x_1, \dots, x_n)$  to a sequence of continuous dense representations  $z = (z_1, \dots, z_n)$ . Given  $z$ , the decoder then generates an output sequence  $y = (y_1, \dots, y_m)$  via one-to-many decoding, as shown in Figure 3. At each step  $t$ , the decoder [19] consumes the previously generated symbols as additional input when generating the next.

**The Transformer** follows this overall architecture using stacked self-attention and point-wise, fully connected layers for both the encoder and decoder, shown in the left and right halves of Figure 1 respectively.

## 3.17. Encoder and Decoder Stacks

**Encoder** and **decoder** stacks have an encoder-decoder structure [26, 10].

Here, the encoder maps an input sequence of symbol representations  $(x_1, \dots, x_n)$  to a sequence of continuous dense representations  $z = (z_1, \dots, z_n)$ . Given  $z$ , the decoder then generates an output sequence  $y = (y_1, \dots, y_m)$  via one-to-many decoding, as shown in Figure 3. At each step  $t$ , the decoder [19] consumes the previously generated symbols as additional input when generating the next.

**The Transformer** follows this overall architecture using stacked self-attention and point-wise, fully connected layers for both the encoder and decoder, shown in the left and right halves of Figure 1 respectively.

## 3.18. Encoder and Decoder Stacks

**Encoder** and **decoder** stacks have an encoder-decoder structure [26, 10].

Here, the encoder maps an input sequence of symbol representations  $(x_1, \dots, x_n)$  to a sequence of continuous dense representations  $z = (z_1, \dots, z_n)$ . Given  $z$ , the decoder then generates an output sequence  $y = (y_1, \dots, y_m)$  via one-to-many decoding, as shown in Figure 3. At each step  $t$ , the decoder [19] consumes the previously generated symbols as additional input when generating the next.

**The Transformer** follows this overall architecture using stacked self-attention and point-wise, fully connected layers for both the encoder and decoder, shown in the left and right halves of Figure 1 respectively.

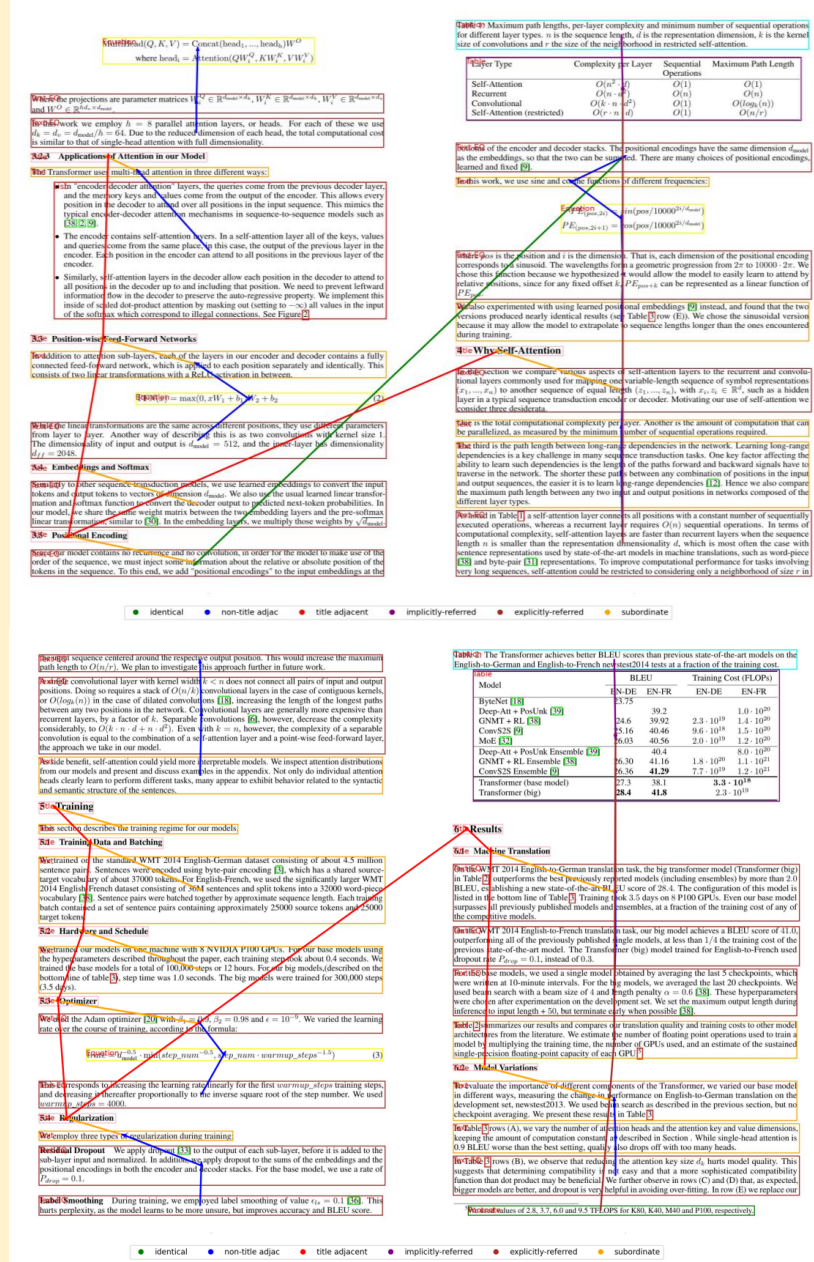
Page 3 of 10

Page 4 of 10

Figure A.5: Annotations of a complete document in DocGenome, taking ‘Attention is All Your Need’ [41] as an example.

# Visualization of Annotations in DocGenome

Page 5 of 10



Page 6 of 10

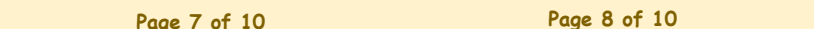
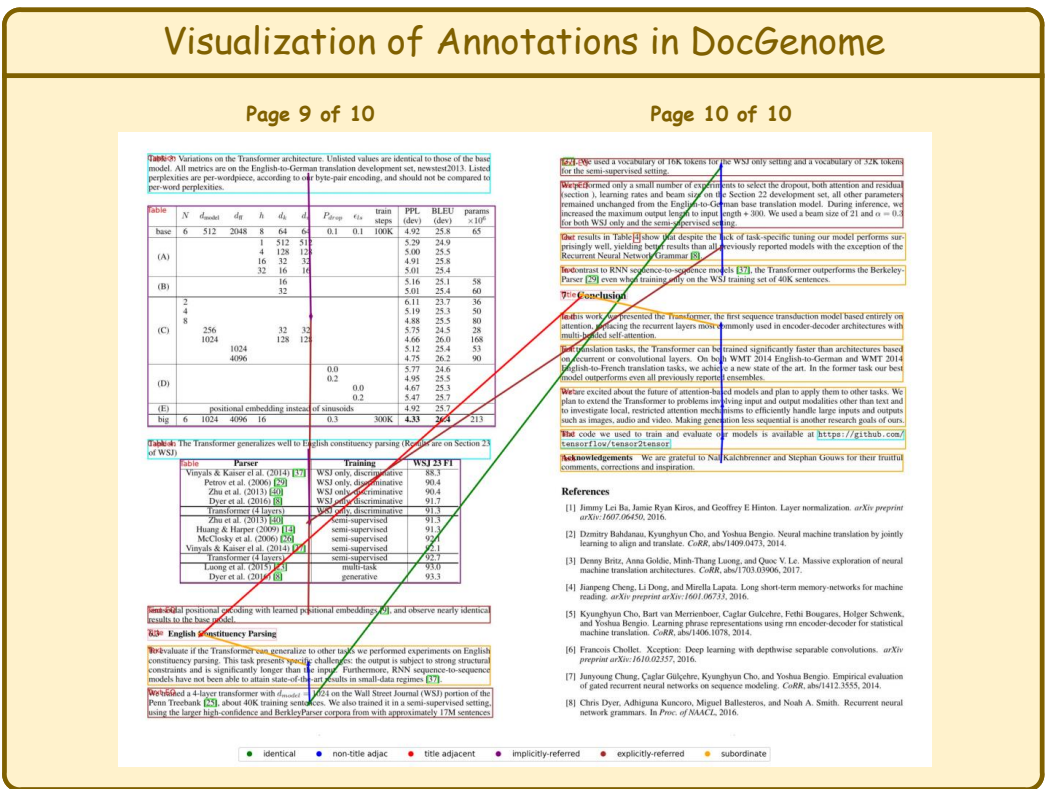
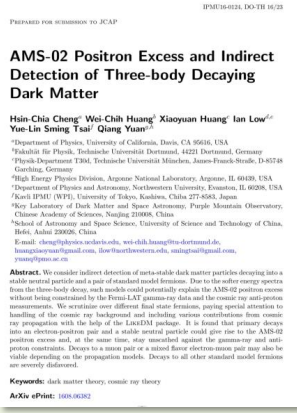


Figure A.6: Annotations of a complete document in DocGenome, taking ‘Attention is All Your Need’ [41] as an example.



## 7 Tasks in DocGenome-test



### 1. Document Classification

Q: Which discipline does this article belong to? Select the answer from the given options (quant-ph, physics.hist-ph, cs.CL, math.PR).

A: quant-ph

### 2. Visual Grounding

Q: Please print the full content of the abstract section of this article.

A: We consider indirect detection of meta-stable dark matter particles decaying into astable neutral particle and a pair of standard model fermions. Due to the softer energy

### 3. Layout Detection

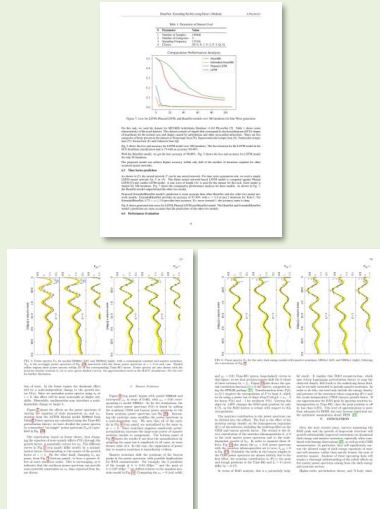
Title: [232, 448, 1416, 672]

Abstract: [230,1430, 1469,1877]

### 4. Single-page QA

Q: What is the best result achieved by the HeunNet model for ECG heartbeat classification?

A: 98.80%



### 5. Multi-page QA

Q: According to Figure 5, what are the shaded yellow regions indicative of in the power spectra  $P_{cb}$  for models M000n1 and M000n2?

A: They show power spectra within 2% of the corresponding Time-RG curves.

### 6. Equation to LaTeX

$$\begin{aligned} \| \mathbf{A} - \mathbf{Q}_1 \mathbf{M} \mathbf{Q}_2^T \|_F^2 &= \| \mathbf{A} - \mathbf{Q}_1 \mathbf{Q}_1^T \mathbf{A} \mathbf{Q}_2 \mathbf{Q}_2^T \\ &+ \mathbf{Q}_1 \mathbf{Q}_1^T \mathbf{A} \mathbf{Q}_2 \mathbf{Q}_2^T - \mathbf{Q}_1 \mathbf{M} \mathbf{Q}_2^T \|_F^2 \\ &= \| \mathbf{A} - \mathbf{Q}_1 \mathbf{Q}_1^T \mathbf{A} \mathbf{Q}_2 \mathbf{Q}_2^T \|_F^2 + \| \mathbf{Q}_1^T \mathbf{A} \mathbf{Q}_2 - \mathbf{M} \|_F^2. \end{aligned} \quad (15)$$

$$\begin{aligned} \| \mathbf{A} - \mathbf{Q}_1 \mathbf{M} \mathbf{Q}_2^T \|_F^2 &= \| \mathbf{A} - \mathbf{Q}_1 \mathbf{Q}_1^T \mathbf{A} \mathbf{Q}_2 \mathbf{Q}_2^T \\ &+ \mathbf{Q}_1 \mathbf{Q}_1^T \mathbf{A} \mathbf{Q}_2 \mathbf{Q}_2^T - \mathbf{Q}_1 \mathbf{M} \mathbf{Q}_2^T \|_F^2 = \| \mathbf{A} - \mathbf{Q}_1 \mathbf{Q}_1^T \mathbf{A} \mathbf{Q}_2 \mathbf{Q}_2^T \|_F^2 \\ &+ \| \mathbf{Q}_1 \mathbf{Q}_1^T \mathbf{A} \mathbf{Q}_2 \mathbf{Q}_2^T - \mathbf{Q}_1 \mathbf{M} \mathbf{Q}_2^T \|_F^2 = \| \mathbf{A} - \mathbf{Q}_1 \mathbf{Q}_1^T \mathbf{A} \mathbf{Q}_2 \mathbf{Q}_2^T \|_F^2 + \| \mathbf{Q}_1^T \mathbf{A} \mathbf{Q}_2 - \mathbf{M} \|_F^2. \end{aligned}$$

| Model              | L1      | MS-SSIM | Inception | FID   |
|--------------------|---------|---------|-----------|-------|
| Internal benchmark |         |         |           |       |
| Non-exemplar       | 0.018   | 5.05E-2 | 3.96      | 11.27 |
| Reference          | 0.014   | 3.97E-2 | 3.82      | 7.67  |
| Code               | 0.015   | 4.15E-2 | 3.94      | 8.49  |
| Celeb-ID           |         |         |           |       |
| Non-exemplar       | 7.36E-3 | 8.44E-3 | 3.72      | 15.30 |
| Reference          | 7.15E-3 | 7.97E-3 | 3.56      | 15.66 |
| Code               | 7.00E-3 | 7.80E-3 | 3.77      | 14.62 |

### 7. Table to LaTeX

```
\begin{table}
\begin{array}{|l|c|c|c|c|} \hline
 & Model & L1 & MS-SSIM & Inception & FID \\ \hline
 & Internal benchmark & & & & \\ \hline
 \multicolumn{6}{|c|}{Non-exemplar} \\ \hline
 & 0.018 & 5.05E-2 & 3.96 & 11.27 & \\ \hline
 \multicolumn{6}{|c|}{Reference} \\ \hline
 & 0.014 & 3.97E-2 & 3.82 & 7.67 & \\ \hline
 \multicolumn{6}{|c|}{Code} \\ \hline
 & 0.015 & 4.15E-2 & 3.94 & 8.49 & \\ \hline
 \multicolumn{6}{|c|}{Celeb-ID} \\ \hline
 \multicolumn{6}{|c|}{Non-exemplar} \\ \hline
 & 7.36E-3 & 8.44E-3 & 3.72 & 15.30 & \\ \hline
 \multicolumn{6}{|c|}{Reference} \\ \hline
 & 7.15E-3 & 7.97E-3 & 3.56 & 15.66 & \\ \hline
 \multicolumn{6}{|c|}{Code} \\ \hline
 & 7.00E-3 & 7.80E-3 & 3.77 & 14.62 & \\ \hline
\end{array}
\end{table}
```

Figure A.8: Visualization examples of 7 tasks in DocGenome-test.